Electron-electron interaction studied in strong central fields by resonant transfer and excitation with H-like U ions

X. Ma,[1,2,*] P. H. Mokler,[1,†] F. Bosch,[1] A. Gumberidze,[1] C. Kozhuharov,[1] D. Liesen,[1] D. Sierpowski,[3] Z. Stachura,[4] Th. Stöhlker,[1] and A. Warczak[3]

[1]*GSI (Gesellschaft für SchwerIonenforschung), Darmstadt, Germany,*
[2]*Institute of Modern Physics, 730000 Lanzhou, China,*
[3]*Jagiellonian University, Institute of Physics, Krakow, Poland*
[4]*Institute of Nuclear Physics, Krakow, Poland*

(Received 23 May 2003; published 23 October 2003)

Electron-electron interaction is studied in the strongest possible atomic fields ($Z\alpha \Rightarrow 1$) in the presence of only two electrons. A quasifree electron from a hydrogen gas target is resonantly captured into an L_j subshell of a fast H-like U^{91+} ion by simultaneous excitation of the strongly bound K electron also into an $L_{j'}$ subshell of the projectile, with j and j' the total angular momenta of 1/2 or 3/2 for the electron of concern. This resonant transfer and excitation process (RTE) $KL_jL_{j'}$ is mediated by electron-electron interaction. It is equivalent to dielectronic recombination in ion-electron collisions and leads to a doubly excited He-like U^{90+}** ion, which stabilizes—almost exclusively—via the emission of two successive K x rays, first a K hypersatellite ($K\alpha_i$-H) and then a K satellite ($K\alpha_{i'}$-S) transition. The K x-ray emission characteristics associated with one-electron capture in collisions of U^{91+} ions with a hydrogen target are studied for the three resonance groups of the $KL_jL_{j'}$ RTE and one off-resonance energy, i.e., in the energy range between 100 and 135 MeV/u. The total cross section for the first resonance group $KL_{1/2}L_{1/2}$ confirms the importance of the Breit contribution to the interaction. The angular distribution for the $K\alpha_2$-H transition ($j=1/2$) is isotropic in the projectile system, whereas the $K\alpha_1$-H transition ($j=3/2$) indicates a strong alignment for the 3/2 electrons in the doubly excited states for the second resonance group $KL_{1/2}L_{3/2}$. The experimental results are in agreement with fully relativistic calculations including the generalized Breit interaction.

DOI: 10.1103/PhysRevA.68.042712 PACS number(s): 34.70.+e, 32.30.Rj, 31.25.−v

INTRODUCTION

Recombination processes governed by electron-electron interaction—the so called dielectronic recombination (DR)—are of great importance in all plasmas from those of stellar origin to laser-induced plasmas [1], for x-ray lasers [2], as well as for accelerator physics, in particular with highly charged heavy ions [3]. DR was first observed as mysterious dielectronic satellite lines in the solar optical spectrum and in 1964 explained theoretically by Burgess [4]. The first step of DR, resonant electron capture, involves two electrons and forms a doubly excited ion, which subsequently stabilizes radiatively. The first part is just the time-reversed Auger process mediated by the electron-electron interaction. In contrast to the Auger process, normally observed in singly ionized low-Z atoms, DR reflects the electron-electron interaction for highly charged ions. Hence, DR has been extensively studied for heavy few-electron ions in recent years; see, e.g., Ref. [5]. This kind of research was also promoted because of the possibilities arising with the advent of cooler electron targets at ion storage rings.

For heavy ionic systems the Breit interaction starts to play a dominant role [6–8]. In extreme cases, the reaction rates increase even by an order of magnitude compared to the pure Coulomb interaction [6]. Unfortunately, for heavy atomic systems the innermost electrons—the K electrons, which probe the strongest possible electric fields [9]—are presently difficult to access by DR measurements at cooler storage rings. In order to excite a K electron of a heavy ion, for instance, to the L shell under resonant capture of a free electron (assuming also to the L shell), high electron energies with respect to the ion are needed. To date, such large detuning energies have not been provided at electron cooler targets. However, atomically confined quasifree target electrons can provide the necessary kinetic energies for those $KL_jL_{j'}$ resonances. Here, we use the Auger notation with j and j' the total angular momenta of the electrons in the created doubly excited state. The doubly excited ion can stabilize radiatively under the emission of the corresponding K x rays, which is the second step in this resonant transfer and excitation process (RTE). Compared to DR involving free electrons, which are magnetically confined by the cooler solenoid, the RTE resonances are smeared out by the Compton profile of the atomically confined electrons. For very heavy ions the radiative stabilization is so fast that it dominates the normally competing Auger decay. Recently, progress toward direct KLL DR measurements has been made at the ESR storage ring using stochastic ion beam cooling and the ''cooler'' as the pure electron target [10]. However, due to geometrical restrictions at cooler targets the photon emission, in particular its emission characteristics, is not accessible in DR measurements.

For very heavy projectiles, measurements of $KL_jL_{j'}$ RTE have been reported from the BEVALAC at Berkeley, Cali-

*Electronic address: X.Ma@GSI.de
†Electronic address: P.Mokler@GSI.de

fornia, for He-like U^{90+} ions colliding with electrons initially confined in C atoms [11] and then—more successfully—in H_2 molecules [12] by measuring just the excitation function for the charge exchange cross sections. Due to the large spin-orbit splitting, three resonance groups for the three different combinations of the total angular momenta j and j' (of 1/2 or 3/2) in the K-shell excited Li-like $U^{89+}*$ could be resolved by RTE measurements. For lighter ions the three $KL_jL_{j'}$ RTE subgroups merge together into one broad KLL resonance group (cf., e.g., [13]). Differential investigations with the heaviest ion—He-like U^{90+}—were performed later at SIS in Darmstadt, measuring the charge exchange in coincidence with the radiative stabilization, i.e., with the characteristic K x-ray emission [14–16]. The x-ray transitions associated with the different j levels could be resolved, giving access to the different total angular momenta involved in the K-shell excited Li-like $U^{89+}*$ states. Moreover, the measured emission characteristics gave access to the alignment of the excited states [17]. In accordance with fully relativistic calculations [18], the Breit term will enhance the cross section for the first resonance group ($KL_{1/2}L_{1/2}$) roughly by an overall factor of 2. Moreover, the Breit interaction influences the magnetic substate population; in the second resonance group ($KL_{1/2}L_{3/2}$) electrons with $j=3/2$ are strongly aligned perpendicular to the ion flight direction. Theoretical studies of the alignment of doubly excited states created by DR (or RTE) show a considerable variation over atomic systems. In particular, the alignment varies with the strength of the probed central field [18,19].

We report here in detail a measurement of the heaviest available, most simply accessible atomic system where an electron-electron interaction can occur: a one-electron (H-like) U^{91+} ion captures by resonant excitation a quasifree target electron atomically confined in a H_2 molecule [20]. In this $KL_jL_{j'}$ RTE process only two electrons are involved and the H_2 gas target used provides the narrowest Compton profile available. Once more, the RTE process is determined via coincidences between the stabilizing characteristic x-ray emission and the associated single-electron capture events. Moreover, the complete x-ray emission pattern is measured in order to extract information on the alignment of the intermediately formed doubly excited states of He-like $U^{90+}**$. In contrast to Li-like ions with a single K-shell excitation as we have it in $U^{89+}*$ ions, for doubly exited He-like ions like $U^{90+}**$ two K vacancies exist with the subsequent emission of a cascade of two characteristic K x rays, the first K x ray being a hypersatellite (''$K\alpha_i$-H'') transition and the second one a satellite (''$K\alpha_{i'}$-S'') transition ($i,i'=1,2$). Due to the screening of the nuclear charge by the first electron filling the K shell, the second transition—the $K\alpha_{i'}$-S transition—has a slightly lower transition energy than the first one, the $K\alpha_i$-H transition. Both transitions $K\alpha_i$-H and $K\alpha_{i'}$-S can be resolved energetically with conventional solid-state x-ray detectors. The advantage of observing $K\alpha_i$-H transitions is that the competing radiative electron capture (REC) process (see, e.g., [21]) cannot produce hypersatellites in the initially H-like ions. The K x-ray cascades $K\alpha_i$-H–$K\alpha_{i'}$-S associated with one-electron capture are measured for the three

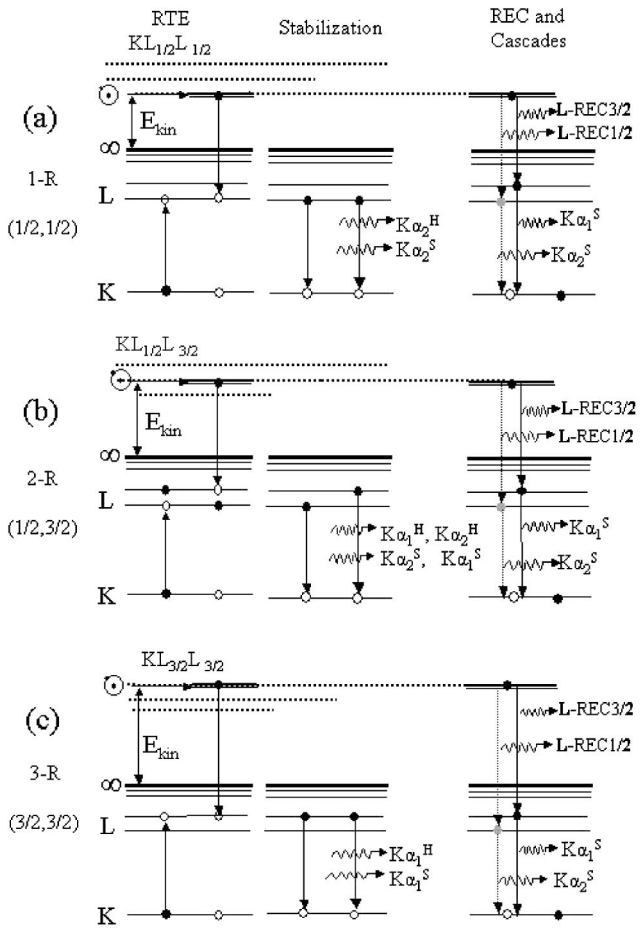

FIG. 1. Explanation of the KL_jL_j RTE process; the level diagrams on the right hand side give the competing L_j REC process for comparison.

$KL_jL_{j'}$ RTE resonance groups (1-R, 2-R, and 3-R corresponding to $KL_{1/2}L_{1/2}$, $KL_{1/2}L_{3/2}$, and $KL_{3/2}L_{3/2}$ RTE) and one off-resonance energy (O-R) in the energy range between 100 and 135 MeV/u. In the preceding paper by Zakowicz *et al.* [22], a fully relativistic description of the RTE processes relevant to this experiment is given, and the calculations are compared with the experimental results presented here.

FORMATION AND DECAY OF DOUBLY EXCITED $U^{90+}**$

The resonant formation of a doubly excited state and its subsequent radiative stabilization is the fingerprint of the RTE process. For the three possible resonance groups in $KL_jL_{j'}$ RTE, the formation and radiative stabilization by a $K\alpha_i$-H–$K\alpha_{i'}$-S x-ray cascade is exemplified in Figs. 1(a)–1(c). On the left side in each case the formation of the doubly excited states is sketched, then in the middle the stabilizing $K\alpha_i$-H–$K\alpha_{i'}$-S x-ray cascade, and for comparison on the right side the competing REC process. Figure 1(a) gives the case for $KL_{1/2}L_{1/2}$ RTE, the first resonance group 1-R: Only $K\alpha_2$-H–$K\alpha_2$-S radiation can be emitted, i.e., only transitions originating from a $j=1/2$ L sublevel, the $K\alpha_2$-H and $K\alpha_2$-S lines, can be observed. $K\alpha_2$-S transitions can also be

caused by REC to the $L_{1/2}$ subshell and its cascade down to the K shell. Similarly, REC to the $L_{3/2}$ level is possible, producing in the end a $K\alpha_1$-S cascade line ($L_{3/2}$ to K transition). A hypersatellite line cannot be produced by REC. However, for the resonance case considered the centroid energy of the broad $L_{1/2}$ REC x-ray distribution coincides with the $K\alpha_2$-H line. Fortunately, the two contributions can be separated via the huge difference in their widths, assuming no interference between RTE and REC. The narrow $K\alpha_2$-H line will stick out of the broad $L_{1/2}$ REC x-ray distribution (cf. Fig. 4 below).

Similar arguments hold true for the second RTE group 2-R, the $KL_{1/2}L_{3/2}$ resonances. From the RTE process, levels with both j values 1/2 and 3/2 are populated simultaneously; see Fig. 1(b). Consequently, the first K x ray can be either a $K\alpha_2$-H or a $K\alpha_1$-H transition (starting with a 1/2 or 3/2 L electron), and the second K x-ray is then a $K\alpha_1$-S or a $K\alpha_2$-S, respectively. Here the satellite lines $K\alpha_1$-S and $K\alpha_2$-S can also be produced as cascade lines from $L_{3/2}$ and $L_{1/2}$ REC, respectively. In the same way we find underneath the sharp hypersatellite lines $K\alpha_2$-H and $K\alpha_1$-H the corresponding broad $L_{3/2}$ and $L_{1/2}$ REC x-ray distributions.

For the third resonance group 3-R, corresponding to $KL_{3/2}L_{3/2}$ RTE, both the electrons in the doubly excited states are in $j=3/2$ levels. Consequently, we observe due to RTE only the $K\alpha_1$-H–$K\alpha_1$-S cascade. The competing $L_{3/2}$ REC will contribute via the cascade to the $K\alpha_1$-S transition, and the broad $L_{3/2}$ REC x-ray distribution will lie under the sharp $K\alpha_1$-H line of the RTE process. Obviously, we will also observe the $L_{1/2}$ REC and its $K\alpha_2$-S cascade line.

Naturally, the x-ray emission associated with the REC process can be studied undisturbed from RTE at an off-resonance energy O-R. Assuming no interference between RTE and REC, the REC contributions found O-R can be used to disentangle the RTE and REC contributions at the different resonance groups. For the measurements described below with initial H-like U^{91+} ions, we used energies of 102.0 MeV/u for O-R, 116.6 MeV/u for 1-R, 124.9 MeV/u for 2-R, and 133.1 MeV/u for 3-R. The resonance energies were calculated using the total binding energies for the corresponding resonance groups with the help of the GRASP structure program [23], and were taken from Ref. [24].

EXPERIMENTAL ARRANGEMENT

The experiment was performed at the heavy-ion accelerator facility of GSI in Darmstadt, Germany. U ions were accelerated by the heavy-ion synchrotron SIS to specific energies of about 280 MeV/u. After stripping in a copper foil, H-like ions were injected into the storage ring ESR, cooled there by merging with a cold electron beam, and then decelerated in the ESR down to the required energies (102.0, 116.6, 124.9, and 133.1 MeV/u). At the measuring energies, the ion beam was energetically fixed and cooled again by electron cooling. On cooling the beam diameter shrank, and the ion beam with its diameter of about 2 mm intersected a H_2 gas jet target. The H_2 gas and the nozzle of the jet target were precooled to liquid nitrogen temperature in order to achieve high target densities through cluster formation. The areal densities ranged up to about 10^{12} H/cm^2. For details of the gas jet arrangement, see [25].

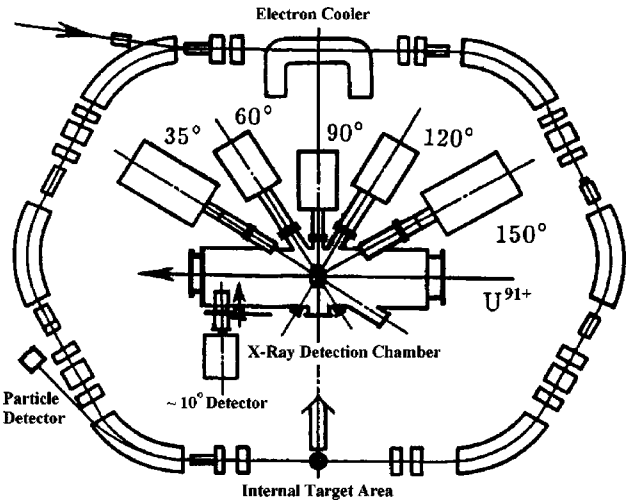

FIG. 2. Experimental arrangement at the heavy-ion storage cooler ring ESR. The inset in the center gives details of the x-ray detection chamber around the gas jet target area.

U^{90+} ions—having captured one electron in the gas jet target—were separated from the circulating U^{91+} ions in the next downstream bending magnet of the ESR and detected behind it in a particle detector inserted into a movable pocket with a thin (50 μm) stainless steel window [26]. For the general layout of the arrangement see Fig. 2. For particle detection a position-sensitive fast gas counter was used. Around the gas jet a photon detection chamber is installed giving access to observation angles in the laboratory frame near 10° and of 35°, 60°, 90°, 120°, and 150°; for details see [27]. The photon detection chamber is equipped for x-ray observation with thin 50 μm stainless steel and 100 μm Be windows at forward and backward observation angles, respectively. The x-ray detection chamber is inserted with an enlarged scale in the center of Fig. 2. For x-ray detection, standard solid state Ge(i) detectors were used with collimators in front of them in order to reduce the angular energy dispersion caused by the Doppler effect. The 10° detector was a special one, segmented into four parallel stripes facing sideways and giving access to four adjacent angles—only two of them were used during the experiment; here, no collimation was needed. Solid angles were calculated from the geometry of the arrangement (yielding values of 1.4, 1.4, 0.88, 0.42, 0.34, and 0.17×10^{-3} sr for the angles from 10° to 150°); detector efficiencies were determined using calibrated radioactive sources.

The emitted x rays were recorded in coincidence with the down-charged U^{90+} ions in event mode using standard electronic modules for signal processing and data acquisition. In Fig. 3, typical raw coincident x-ray spectra taken at 150° for the four measuring energies (O-R, 1-R, 2-R, and 3-R) are shown in a three-dimensional representation. For convenience, the x-ray energies are already transformed into the emitter frame of the ion. The identifications of the lines are sketched in the projection plane at the top of the figure. For the off-resonance case (O-R), we see only the broad $L_{3/2}$ and

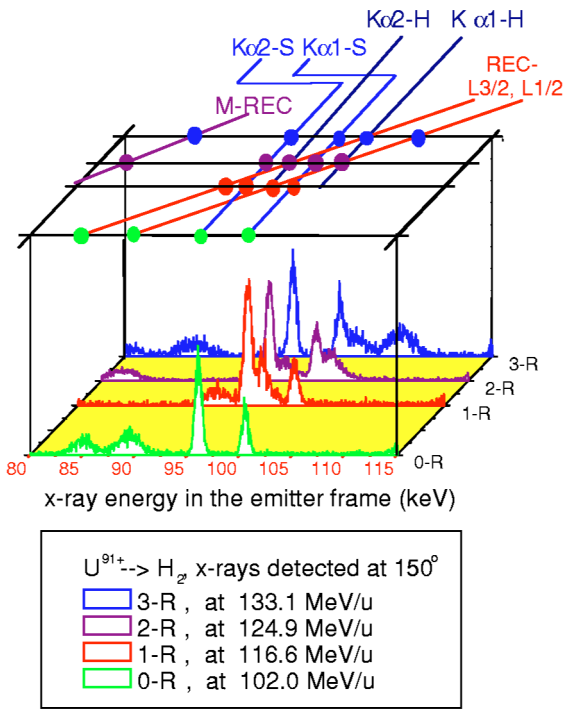

FIG. 3. (Color online) X-ray spectra associated with one electron capture for U^{91+} on H_2 at 102.0 MeV/u (O-R), 126.6 MeV/u (1-R), 124.9 MeV/u (2-R), and 133.1 MeV/u (3-R) taken at an observation angle of 150°. In the plane at the top of the figure the different transitions are indicated.

$L_{1/2}$ REC lines (around 85.0 and 89.4 keV) and the sharp cascade contributions $K\alpha_2$-S and $K\alpha_1$-S (at about 96.2 and 100.6 keV). With an increase in ion energy the broad L REC lines shift successively to higher x-ray energies for the resonance groups 1-R, 2-R, and 3-R, respectively. For group 1-R the $L_{1/2}$ REC line coincides with the narrow $K\alpha_2$-H line (at 97.5 keV) caused by RTE; for group 2-R the $L_{1/2}$ REC line already coincides with the $K\alpha_1$-H line (at 101.9 keV) from RTE and the $L_{3/2}$ REC with the $K\alpha_2$-H line from RTE. And, finally, for group 3-R there is no $K\alpha_2$-H line, the $L_{3/2}$ REC coincides with the $K\alpha_1$-H from RTE, and the $L_{1/2}$ REC contribution is already outside the region of interest. For the two high ion energy spectra for groups 2-R and 3-R, the REC contributions to the M shell show up on the low x-ray energy side.

At the other observation angles the spectra look quite similar. However, due to the strong variation of the angular distribution for the broad REC radiation [28] the visibility of the $K\alpha_i$-H lines changes with angle. The REC contributions are especially strong around observation angles of 90°.

DECOMPOSITION OF SPECTRA

The 28 x-ray spectra taken at the different ion energies and at all the observation angles were decomposed into the various contributions using Gaussian distributions for the lines and a linear background subtraction. The linewidths for the broad REC lines as well as their intensity ratio were fixed according to expectation whenever it was necessary for the fitting routine. Here, the O-R spectra give a good starting value. Different fitting routines were used, applying also standard response line shapes for the lines of the K x-ray transitions and appropriately broader distributions for the REC contributions. At the statistical level available, however, no real variance in the result could be observed. So in the following we stick to the decomposition of the spectra using Gaussian line distributions. The negligible variance in the different methods for spectra deconvolution gives us confidence that there are only small systematic errors of our analysis.

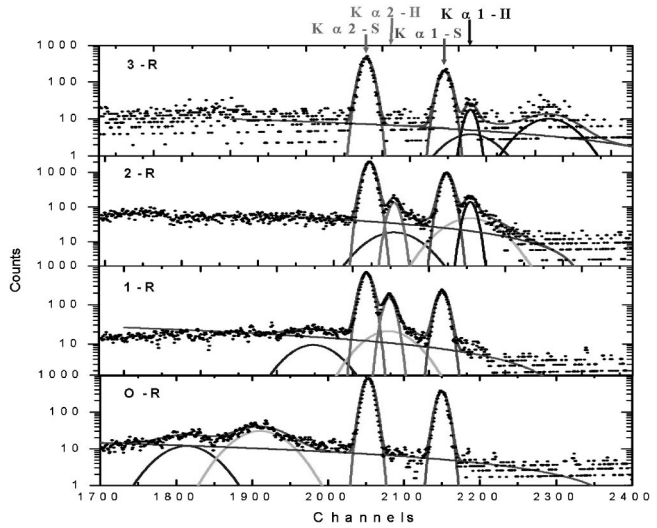

FIG. 4. Decomposition of the L x-ray spectra into the various components. The channels have been shifted in such a way that characteristic lines are aligned visually.

Examples of the decomposition of the spectra are given in Fig. 4 for the four ion energies at O-R, 1-R, 2-R, and 3-R for one observation angle of 14.7°. In the spectra the true counts per channel are given in order to be able to judge the statistics. Due to the Doppler effect the lines shift in channel for the different ion energies; for convenience in the representation we adjust the spectra in such a way that the main characteristic K lines stay at the same position. In the semilogarithmic plot the different contributions are clearly visible. As mentioned already, the L REC lines shift with increasing ion energy to higher x-ray energies: for group 1-R the broad $L_{1/2}$ REC distribution is right under the narrow $K\alpha_2$-H line, for group 2-R both the L_j REC contributions are under both the hypersatellite lines $K\alpha_i$-H, and finally for group 3-R the $L_{3/2}$ REC part shifts under the $K\alpha_1$-H line.

From the decomposition of the spectra we obtain relative line intensities for each spectrum. These relative line intensities are summarized in Table I for all the observation angles and all the ion energies used. For the convenience of the reader detector efficiencies have already been incorporated into the numbers given. Hence, after incorporating the solid angles the intensities for one ion energy will give the relative angular differential cross sections in the laboratory system. Additionally, these values still have to be normalized to the reaction product of the number of ions times the target den-

TABLE I. Relative line intensities (for details see text).

Θ_{lab} (deg)	K REC	$L_{3/2}$ REC	$L_{1/2}$ REC	$K\alpha_2$-S	$K\alpha_1$-S	$K\alpha_2$-H	$K\alpha_1$-H	K REC theory (b/sr)
Off resonance at 102.0 MeV/u								
13.3	1876	729	1808	11641	5369			3.02
14.7	1934	862	2102	11347	5012			3.21
35	4972	432	3757	9819	4195			7.41
60	6753	965	3148	4455	1948			12.69
90	3123	796	1517	1375	573			13.83
120	2155			839	321			9.04
150	2600	944	1459	2289	1088			2.79
Resonance group 1 at 116.6 MeV/u								
13.3	1335	2569	1578	9964	3490	2618		2.64
14.7	1266	2353	1335	9742	3355	2314		2.80
35	3449	1803	1803	8983	2771	1803		6.31
60	4707	1102	1962	3866	1265	1102		10.77
90	2312	251	251	1037	368	251		11.72
120	1598							7.65
150	1683	445	445	1946	685	445		2.35
Resonance group 2 at 124.9 MeV/u								
13.3	4355	940	2332	30002	13506	2246	2059	2.46
14.7	4897	1037	2529	29197	13471	2092	2249	2.61
35	12042							5.81
60	17304	2282	7446	10529	4771	535	1579	9.89
90	7813	1465	2791	3085	1485	133	438	10.76
120	5600							7.02
150	5537	2171	3356	5161	2509	413	513	2.16
Resonance group 3 at 133.1 MeV/u								
13.3	1032	265	657	7048	3224		311	2.31
14.7	1006	262	640	6859	3076		272	2.44
35	2994							5.37
60	4463	532	1735	2420	1087		72	9.13
90	2112							9.93
120	1287							6.47
150	1339	556	859	1086	558		44	2.00

sity and measuring time. In order to get absolute cross sections, we have to normalize the $K\alpha$ line intensities to the K REC line that shows up at higher x-ray energies. The K REC radiation was separately registered in coincidence with capture events using a second set of main amplifiers with lower amplification. Additionally, the K REC intensities—also corrected for efficiency—are given in Table I. By applying this normalization procedure, all the systematic errors are canceled in the cross section calculations. The K REC radiation is preferentially emitted perpendicular to the ion beam direction [29,30], and its angular distribution has to be taken into account. On the other hand, normalizing the 90° data to the K REC is sufficient if for the other angles the solid angle corrections are included in the numbers given in Table I. For completeness we add in the last column the theoretical angular differential cross sections for K REC per K vacancy in U^{92+} as calculated by Eichler and co-workers [31,32].

EXPERIMENTAL RESULTS AND DISCUSSION

As the $K\alpha_2$-S line is a 1/2-to-1/2 transition, on a first glance we may expect an isotropic emission pattern in the emitter frame. However, in reality we have to consider the total angular momenta involved for the relevant two-electron states [22]. In Fig. 5 the angular differential $K\alpha_2$-S x-ray emission cross sections as observed in the laboratory system ($d\sigma_{K\alpha_2\text{-}S}/d\Omega_{lab}$) are plotted for the off-resonance case (O-R). Due to the Lorentz transformation the emission in the laboratory system is strongly forward peaked and coincides perfectly with an isotropic emission pattern in the moving ion system (emitter system) transformed into the laboratory frame. In the lower part of the figure the ratio of the data to the expectation of the Lorentz transformation ($K\alpha_2$-S/Lorentz) is plotted, confirming the isotropic emission characteristic.

For the three resonance energies 1-R, 2-R, and 3-R, also

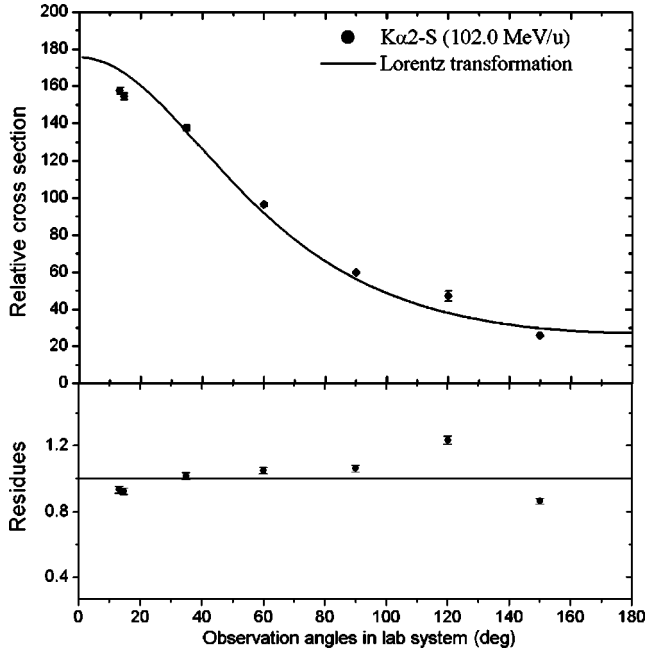

FIG. 5. The emission characteristic of the $K\alpha_2$-S line as observed in the laboratory at the O-R energy of 102.0 MeV/u. The solid line gives the Lorentz transformation for isotropic emission in the emitter frame. At the bottom the ratio $K\alpha_2$-S/Lorentz transformation is given.

the emission patterns for the $K\alpha_2$-S lines are found experimentally to be practically isotropic in the emitter frame of the moving ion; see the corresponding ratios ($K\alpha_2$-S/Lorentz) in Fig. 6. That means that the $K\alpha_2$-S lines display isotropic emission experimentally independent of the ion energies and possibly also independent of the production process—i.e., cascades from RTE or from REC. Considering the strong REC cascade contribution to the $K\alpha_2$-S line, this

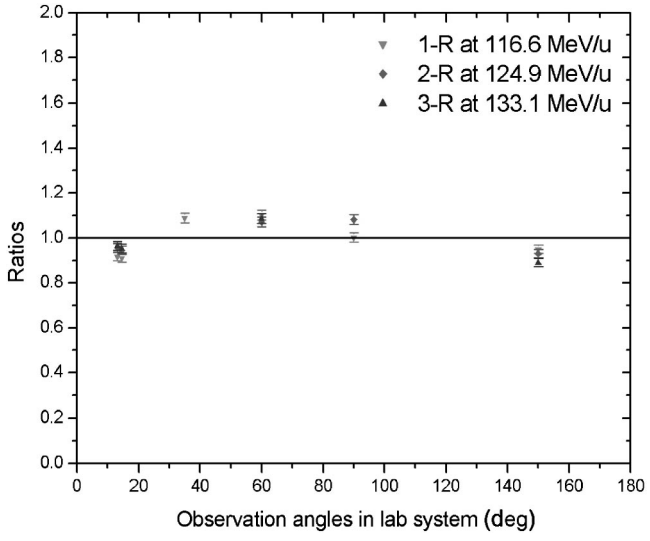

FIG. 6. The ratios for the $K\alpha_2$-S emission to the expectation of isotropic emission in the emitter frame for the three resonance groups 1-R (116.6 MeV/u), 2-R (124.9 MeV/u), and 3-R (133.1 MeV/u).

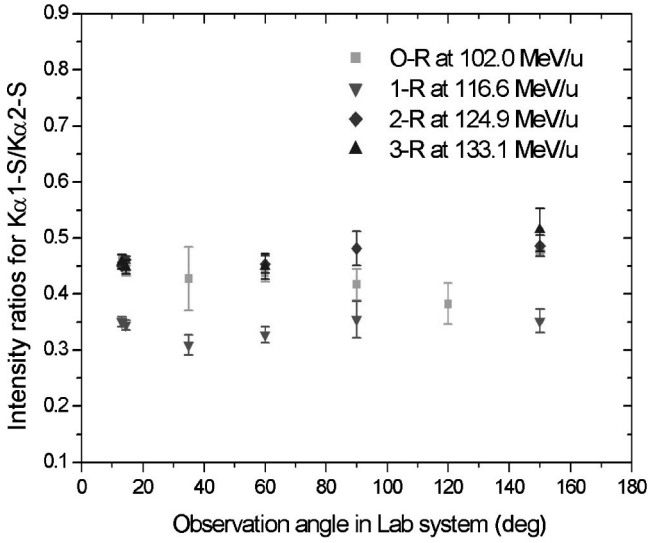

FIG. 7. $K\alpha_1$-S/$K\alpha_2$-S intensity ratios as a function of the emission angle for all the measured cases O-R, 1-R, 2-R, and 3-R.

does not necessarily mean that all the RTE contributions also have to be isotropic: A small anisotropic RTE contribution may not disturb the observed isotropy at the available level of experimental significance (compare Ref. [22]). As the total $K\alpha_2$-S emission is observed to be isotropic, we will use this fact to normalize all our other lines to the $K\alpha_2$-S line. Hence, considering the corresponding line intensity ratios, all solid angle corrections and transformation factors will cancel, and the ratios will just give the emission patterns in the emitter frame (but displayed for the actual observation angles in the laboratory).

The $K\alpha_1$-S line is a 3/2-to-1/2 transition and its emission characteristics may depend on its production mechanisms. In Fig. 7 the ratios $K\alpha_1$-S/$K\alpha_2$-S are plotted for all the measured ion energies O-R, 1-R, 2-R, and 3-R. For all ion energies only negligible anisotropies are observed. However, within the measuring accuracies in all cases the $K\alpha_1$-S emission can also be considered as isotropic. The average values for the $K\alpha_1$-S/$K\alpha_2$-S ratios are about 0.435 ± 0.030 for O-R, 0.340 ± 0.018 for 1-R, 0.466 ± 0.016 for 2-R, and 0.467 ± 0.032 for 3-R. The O-R value is caused only by REC contributions, whereas the ratios at the different resonances in comparison to the off-resonance value give a crude number for the additional relative cascade contributions to the satellite x-ray emission caused by RTE, which will be considered below.

However, first we want to emphasize that for *bare* projectiles a strong anisotropy was observed for the $K\alpha_1$-S emission from pure REC cascades [30], pointing there to a strong alignment for the captured electron. This is in evident contrast to our finding for the H-like projectiles. How far here a coupling to the second electron—we have intermediate two-electron states—influences the emission pattern will be discussed elsewhere.

In contrast to O-R where only REC cascades contribute to the $K\alpha_1$-S/$K\alpha_2$-S emission, for group 1-R RTE also contributes to the $K\alpha_2$-S line and the $K\alpha_1$-S/$K\alpha_2$-S ratio decreases correspondingly. From the experimental value of

0.340 we can extract that the RTE cascade contribution to the $K\alpha_2$-S transition is only a fraction of about 0.28 of the REC contribution. Or, referring to the total line intensity, only about 22% ($=1/4.58$, see below) of the $K\alpha_2$-S line is caused by RTE. This evaluation assumes that the $K\alpha_1$-$S/K\alpha_2$-S ratio caused by REC cascades alone does not change with ion energy.

For the other resonance groups, especially for 2-R, it is difficult to extract directly from the experimental ratios $K\alpha_1$-$S/K\alpha_2$-S the RTE cascade contributions to these lines. However, we can use as additional input the calculated ratios of the RTE cross sections for the different x rays. Hence, we refer to the corresponding theoretical x-ray emission cross sections induced by RTE given in Table II of the preceding paper of Zakowicz *et al.* [22]. (There, the small contributions to $K\alpha_1$-H as well as to $K\alpha_1$-S and to $K\alpha_2$-H as well as to $K\alpha_2$-S in resonance groups 1 and 3, respectively, are due to the overlap from the neighboring resonance groups induced by the Compton profile.)

For the second resonance group 2-R, the $K\alpha_1$-$S/K\alpha_2$-S ratio (0.466) again approaches the off-resonance value (0.435) and overshoots it. This indicates that RTE contributes with a similar fraction to both the satellite lines ($K\alpha_1$-S, $K\alpha_2$-S) showing a tendency to a somewhat higher relative contribution to the $K\alpha_1$-S line. According to the theoretical values [22] the $K\alpha_2$-S emission cross section for the RTE part for group 2-R is only a fraction of 0.41 of that for group 1-R. A similar cross section ratio at both resonances was found experimentally also for the case of initially He-like U ions [14–16]. Assuming for the $K\alpha_2$-S line for group 2-R a RTE cascade contribution equivalent to the one for group 1-R reduced by the corresponding RTE cross section ratio, we find that only about 10.3% ($=1/9.74$) of the $K\alpha_2$-S radiation is caused by RTE. For the $K\alpha_1$-S line we find a relatively higher RTE cascade contribution of about 16%. (Nevertheless, the absolute emission cross section for $K\alpha_1$-S is considerably smaller than that for $K\alpha_2$-S.) Due to the experimental uncertainties all these numbers can only be guidelines.

For the third resonance group 3-R, the $K\alpha_1$-$S/K\alpha_2$-S ratio does not change further within the errors; a RTE cascade contribution to the $K\alpha_2$-S line is not possible here. From this we deduce that RTE contributes only a small part of about 7% to the $K\alpha_1$-S emission. (For comparison, this would correspond to only about 3% of the $K\alpha_2$-S intensity.) We emphasize that the RTE resonance strength for group 3-R is relatively weak.

Hypersatellite lines cannot be caused by REC cascade contributions at all. Hence, these lines give directly the contributions from the RTE process alone. As explained already, for groups 1-R and 3-R we expect contributions to the $K\alpha_2$-H and $K\alpha_1$-H lines, respectively, and for group 2-R both the $K\alpha_2$-H and $K\alpha_1$-H lines. The corresponding ratios $K\alpha_2$-$H/K\alpha_2$-S and $K\alpha_1$-$H/K\alpha_2$-S are shown in Figs. 8 and 9, respectively. The $K\alpha_2$-H is a 1/2-to-1/2 transition, and it is not surprising that the $K\alpha_2$-$H/K\alpha_2$-S ratios display isotropic emission patterns. Theory predicts isotropic emission for $K\alpha_2$-H transitions also [22]. The experimental mean absolute values for the $K\alpha_2$-$H/K\alpha_2$-S ratios are about 0.24

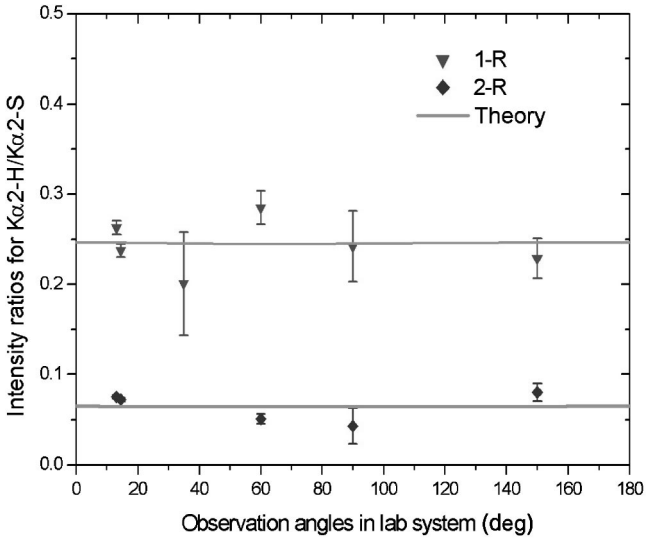

FIG. 8. $K\alpha_2$-$H/K\alpha_2$-S intensity ratios for the first and second RTE resonance groups 1-R and 2-R. The full lines give the theoretical predictions according to Ref. [22].

± 0.03 for group 1-R and 0.064 ± 0.016 for group 2-R. The theoretical ratios calculated from the theoretical emission cross sections given in Ref. [22] are 1.00 and 0.48, respectively. However, the theoretical values do not include the REC cascade contributions and hence have to be divided by the reduction factors quoted above of 4.58 and 9.74, yielding $K\alpha_2$-$H/K\alpha_2$-S ratios of 0.21 for group 1-R and 0.05 for group 2-R. These theoretical predictions for the ratios agree quite nicely within the expected accuracies with the experimental findings (see also Fig. 8).

The $K\alpha_1$-H emission corresponds to transitions from 3/2 to 1/2 states and may show anisotropic behavior due to the alignment caused by the RTE process. Indeed, the $K\alpha_1$-$H/K\alpha_2$-S ratio for the second resonance group 2-R shows a pronounced dipole emission pattern in the emitter

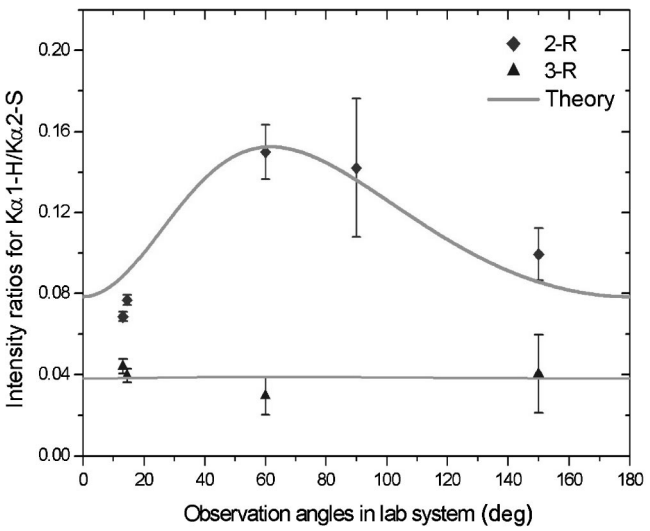

FIG. 9. $K\alpha_1$-$H/K\alpha_2$-S intensity ratios for the second and third resonance groups 2-R and 3-R. The full lines are the theoretical results according to Ref. [22].

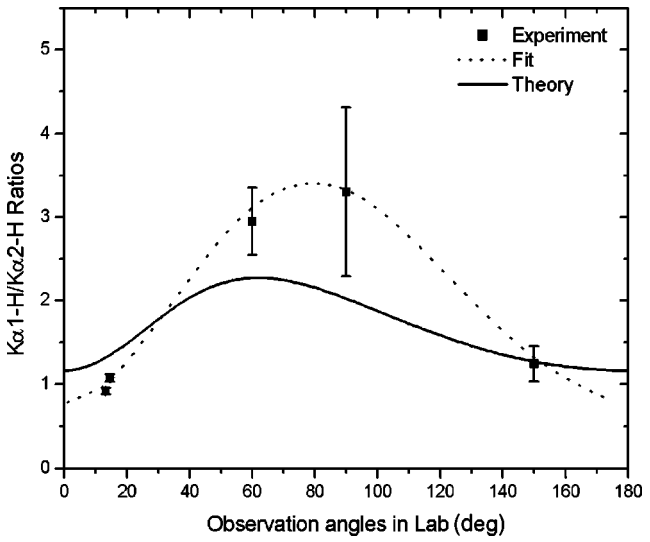

FIG. 10. $K\alpha_1$-H/$K\alpha_2$-H intensity ratios for the second resonance group 2-R. The full lines give the theoretical results according to [22]; the dotted line is a fit to the experimental data.

frame (see Fig. 9). (At these ion energies a lab angle of 60° corresponds roughly to 90° in the emitter system.) From theory [22] we expect an average $K\alpha_1$-H/$K\alpha_2$-S ratio of 0.90 for RTE alone, which once more has to be reduced by a factor of 9.74, yielding a mean ratio of 0.093. This is in good agreement with the mean experimental value around 0.1. Moreover the theoretical expectation for the emission pattern included in Fig. 9 is also in reasonable agreement with the experimental findings. (In the theoretical ratio given here, we neglected the $K\alpha_2$-S contributions from RTE; only the $K\alpha_2$-S intensity caused by REC is used.)

For the resonance group 3-R the $K\alpha_1$-H/$K\alpha_2$-S ratio shows an experimental value of only around 0.04, which has to do with the fact that this resonance strength is pretty small and the REC contributions are correspondingly dominant. The emission pattern seems to be isotropic with a tendency to opposite emission characteristics, possibly pointing to a reversed alignment compared to the second resonance 2-R. Considering only the RTE contributions, we deduce from theory [22] a $K\alpha_1$-H/$K\alpha_2$-S ratio of 6.2, which has here to be reduced roughly by a factor of 30 including REC contributions to the total $K\alpha_2$-S emission. However, this ratio is completely blurred by a huge systematic uncertainty.

As REC does not contribute to the hypersatellite lines at all, for the second resonance group 2-R we can also consider the intensity ratio of the hypersatellites $K\alpha_1$-H/$K\alpha_2$-H, which cannot be disturbed by any REC contributions. Since we showed (in Fig. 8) that the $K\alpha_2$-H line displays an isotropic emission pattern, the $K\alpha_1$-H/$K\alpha_2$-H ratio depicted in Fig. 10 should give directly the emission characteristic of the $K\alpha_1$-H line. This ratio can be compared to theory [22] on an absolute scale, as no reduction factors have to be applied. This absolute comparison (see the full line in Fig. 10) demonstrates an overall good agreement. However, the experimental points may suggest a stronger anisotropy than predicted (see dotted line). This observed stronger anisotropy might be caused by contributions from higher multipole transitions, as in the theoretical treatment only electric dipole transitions have been included. A similar enhancement of the anisotropy caused by higher multipole contributions has been reported for the case of REC cascades for initially bare U^{92+} projectiles [33].

TABLE II. Total hypersatellite emission cross sections (barn per target electron) in comparison to the corresponding RTE cross sections. The theoretical values are from Ref. [22]; the numbers in parentheses give the results of calculations without Breit interaction.

	1-R	2-R		3-R
	$K\alpha_2$-H	$K\alpha_2$-H	$K\alpha_1$-H	$K\alpha_1$-H
Experiment	22.4 ± 2.7	4.5 ± 1.5	7.2 ± 0.8	2.5 ± 0.8
Theory	21.7 (12.0)	4.2 (4.5)	7.9 (7.2)	2.9 (2.4)

From the $K\alpha_1$-H/$K\alpha_2$-H ratios we can extract an anisotropy parameter β_A using

$$W(\theta) \propto 1 + \beta_A \mathcal{P}_2(\cos\theta)$$

(with $\mathcal{P}_2$ the Legendre polynomial). A fit to the data leads to a value of $\beta_A = -0.75$ (see the dotted line in Fig. 10). In a one-electron approximation (H-like system), β_A can vary only between 0.5 and -0.5 for a single electron transition from 3/2 to 1/2 with dipole emission. Couplings to the second electron and possible higher multipole contributions will change this (cf. also [34]). In the preceding paper [22] electron-electron coupling is already included in the calculations; however, no higher multipole contributions are considered. Assuming for the moment the one-electron approximation, i.e., no coupling of the $j=3/2$ electron to the other one with $j=1/2$ and additionally no higher multipole contributions, the alignment A of the magnetic substate population $P_{|mj|}$ (with $|m_j| = 1/2$ and 3/2) would be given by

$$A = (P_{|3/2|} - P_{|1/2|})/(P_{|3/2|} + P_{|1/2|}).$$

For such a dipole emission we have $\beta_A = 0.5A$ (cf. [16]). With $\beta_A = -0.5$ this yields a value for the alignment of $A = -1.0$, which means $|m_j| = 1/2$ substates are preferentially populated in the 3/2 level. Or, in other words, only angular momenta j perpendicular to the collision direction can be transferred for the $j=3/2$ states considered. It is interesting to note that for the third resonance group 3-R where both the electrons are in $j=3/2$ intermediate states the alignment A is zero or even slightly positive (cf. Fig. 9). This may mean that the Pauli exclusion principle in connection with the j-j coupling destroys the alignment completely.

Finally, with the measured emission characteristics for the different lines we can determine the total strengths of the resonances by integrating over all the angles. For absolute normalization the K REC cross sections calculated by Eichler and Ichihara [32] were used. The total RTE cross sections extracted from the hypersatellite contributions are summarized in Table II and compared to the theoretical values determined by the fully relativistic theory [22]. For com-

parison, the cross sections not including the relativistic Breit term are also given in parentheses. For the first resonance group 1-R an appreciable difference between fully relativistic and nonrelativistic calculations has been reported. The experimental values evidently confirm the fully relativistic theory including the complete Breit term for the interaction.

In the data analysis and interpretation given above, we did not use calculated L REC cross sections in order to avoid any ambiguities. However, we wish to stress that the predictions for the total L REC cross sections from [32] agree well with the observed values. In particular, for O-R the measured intensity ratio $K\alpha_1$-$S/K\alpha_2$-S of 0.435 ± 0.030 corresponds nicely to the calculated $L_{3/2}/L_{1/2}$ REC cross section ratio of 0.420. Using the theoretical total L_j REC cross sections, the RTE contributions to the line intensities can be extracted directly. Both REC and RTE calculations agree quite nicely with the experimental findings.

CONCLUSIONS

For the heaviest and simplest atomic system resonant transfer and excitation involving the innermost shells have been investigated. We measured for H-like U^{91+} projectiles the $KL_jL_{j'}$ RTE using a H_2 gas target, providing the narrowest possible Compton profile for atomically confined quasifree target electrons. We studied the emission patterns of the cascade decay of doubly excited He-like U^{90+}** ions where the first hypersatellite ($K\alpha_i$-H) and the second satellite ($K\alpha_{i'}$-S) transitions are energetically separated. Although the REC cascade contributions to the satellite lines ($K\alpha_{i'}$-S) dominate, the RTE contributions could be isolated. In particular, the hypersatellite ($K\alpha_i$-H) transitions are free of REC contributions—neglecting possible small interference effects.

The emission patterns for the satellite lines, for $K\alpha_2$-S as well as for $K\alpha_1$-S, are found to be isotropic. However, these transitions are heavily determined by the REC cascade contributions, which have also been found to be isotropic. The latter is in clear contrast to the emission for REC cascades observed recently with bare U^{92+} projectiles [33]; this point will be considered elsewhere. The anisotropies predicted for the satellite contributions caused by RTE cascades cannot be observed for our case within the experimental uncertainties. However, the hypersatellite emission is free of REC cascade contributions: For the first resonance 1-R ($KL_{1/2}L_{1/2}$ RTE) isotropic emission for the $K\alpha_2$-H emission is found as predicted. For the second resonance group 2-R ($KL_{1/2}L_{3/2}$ RTE) the $K\alpha_1$-H is strongly anisotropic in overall accordance with theory pointing to a complete alignment of the $j=3/2$ electrons. However, the experiment shows a large alignment parameter of $\beta_A = -0.75$, exceeding the predicted value. How far this enhancement may be caused by higher multipole contributions has to be further investigated. For group 2-R, for the $K\alpha_2$-H emission isotropy is observed—possibly with a slight tendency to an opposite anisotropy—and this agrees with predictions. For the third resonance group 3-R ($KL_{3/2}L_{3/2}$ RTE) no anisotropy could be found for the $K\alpha_1$-H emission, also in accordance with theory.

The measured intensity ratios for the prominent x-ray lines also fit the expectations and were used to normalize the RTE cascade contributions to the satellite lines. From the measured angular distributions total cross sections for hypersatellite emission caused by RTE were reported. Normalizing these relative cross sections using the K REC emission gives absolute values that are in agreement with the fully relativistic calculations including the full Breit interaction. For the first resonance group the Breit interaction increases the cross section by a factor of 2. In summary, a general good agreement between fully relativistic theory and experiment can be stated for pure electron-electron interaction in the strongest possible atomic fields. This is true for both the total as well as the angular differential x-ray emission.

ACKNOWLEDGMENTS

Close and good collaboration with our colleagues from the theoretical physics department at the University of Giessen under the leadership of Werner Scheid is highly appreciated; especially we name additionally Stephan Zakowicz, Zoltán Harman, and Norbert Grün. We wish to thank also Jörg Eichler and his colleague Akira Ichihara for providing us with calculations for the REC contributions. We are indebted to the ESR team, Markus Steck and his colleagues, for providing us with an excellent beam, to Otto Klepper for his assistance with the particle detector, to Uli Popp for his help with the gas jet operation, and to the colleagues from the atomic physics group supporting the beam time. Support and grants from EU (No. EC-HPRI-CT-1999-0001 and No. HPMT-CT-2000-00179) and from WTZ, Bairen Plan, and NSFC are gratefully acknowledged.

[1] D.R. Bates, Case Stud. At. Phys. **4**, 62 (1974).
[2] B.L. Whitten, A.U. Hazi, M.H. Chen, and P.L. Hagelstein, Phys. Rev. A **33**, 2171 (1986).
[3] S. Baird *et al.*, Phys. Lett. B **361**, 184 (1995).
[4] A. Burgess, Astrophys. J. **139**, 776 (1964).
[5] C. Brandau *et al.*, Nucl. Instrum. Methods Phys. Res. B **205**, 66 (2003).
[6] P. Zimmerer, N. Grün, and W. Scheid, Phys. Lett. A **148**, 457 (1990).
[7] M.H. Chen, Phys. Rev. A **41**, 4102 (1990).
[8] M.S. Pindzola and N.R. Badnell, Phys. Rev. A **42**, 6526 (1990).
[9] G. Soff *et al.*, Adv. Quantum Chem. **30**, 125 (1998).
[10] C. Brandau *et al.*, Scientific Report 2002, GSI Report No. 2003-1 (unpublished), p. 91, http://www.gsi.de/annrep2002.
[11] J. A. Tanis *et al.*, Nucl. Instrum. Methods Phys. Res. B **53**, 442 (1991).
[12] W.G. Graham *et al.*, Nucl. Instrum. Methods Phys. Res. B **53**, 2773 (1990).
[13] P.H. Mokler and S. Reusch, Z. Phys. D: At., Mol. Clusters **8**,

393 (1988).
[14] T. Kandler *et al.*, Phys. Lett. A **204**, 274 (1995).
[15] T. Kandler *et al.*, Z. Phys. D: At., Mol. Clusters **35**, 15 (1995).
[16] T. Kandler *et al.*, Nucl. Instrum. Methods Phys. Res. B **98**, 320 (1995).
[17] P.H. Mokler *et al.*, Phys. Scr. **T73**, 247 (1997).
[18] M. Gail, N. Grün, and W. Scheid, J. Phys. B **31**, 4645 (1998).
[19] M.H. Chen and J.H. Scofield, Phys. Rev. A **52**, 2057 (1995).
[20] X. Ma *et al.*, Nucl. Instrum. Methods Phys. Res. B **205**, 550 (2003).
[21] Th. Stöhlker *et al.*, Phys. Rev. Lett. **86**, 983 (2001).
[22] S. Zakowicz, Z. Harman, N. Grün, and W. Scheid, preceding papers Phys. Rev. A **68**, 042711 (2003).
[23] K.G. Dyall *et al.*, Comput. Phys. Commun. **55**, 425 (1989).
[24] M. Gail, Ph.D. thesis, University of Giessen, 2000; and (private communication).
[25] A. Krämer, A. Kritzer, H. Reich, and Th. Stöhlker, Nucl. Instrum. Methods Phys. Res. B **174**, 205 (2001).
[26] O. Klepper, Nucl. Phys. A **626**, 199c (1997).
[27] Th. Stöhlker *et al.*, Phys. Rev. Lett. **82**, 3232 (1999).
[28] Th. Stöhlker, P.H. Mokler, C. Kozhuharov, and A. Warczak, Comments At. Mol. Phys. **33**, 271 (1997).
[29] G. Bednarz *et al.*, Nucl. Instrum. Methods Phys. Res. B **205**, 573 (2003).
[30] Th. Stöhlker *et al.*, Phys. Rev. Lett. **79**, 3270 (1997).
[31] A. Ichihara, T. Shirai, and J. Eichler, Phys. Rev. A **54**, 4954 (1996).
[32] J. Eichler and A. Ichihara (private communication).
[33] A. Surzhykov, S. Fritzsche, A. Gumberidze, and Th. Stöhlker, Phys. Rev. Lett. **88**, 153001 (2002).
[34] M. Gail, N. Grün, and W. Scheid, J. Phys. B **31**, 4645 (1998).